[PS]Using B4 LiDAR and CRN Age Data to Constrain Slip Rates Along the San Andreas Fault System at Millard Canyon, San Gorgonio Pass*

Ian Desjarlais[1], Doug Yule[1], and Richard Heermance[1]

Search and Discovery Article #41652 (2015)**
Posted July 20, 2015

*Adapted from poster presentation given at Pacific Section AAPG, SEG and SEPM Joint Technical Conference, Oxnard, California, May 3-5, 2015

[1]California State University, Northridge, CA (ian.desjarlais@csun.edu)

Abstract

Fault scarps cut a series of Holocene alluvial fan surfaces in Millard Canyon, within the San Gorgonio Pass (SGP). These fault scarps are likely the result of coseismic slip along the San Andreas Fault system during potentially large magnitude (Mw7+) earthquakes. Here we provide new ages for Holocene surfaces Qf2, Qf3, and Qf4. Charcoal fragments beneath Qf2 limits the surface to 1270 ± 80 years before present (ybp) and new 10Be exposure ages from the two older Holocene surfaces provide age constraints of 4800 ± 1600 ybp for Qf3 and 6800 ± 550 ybp for Qf4. These new ages provide limits on the timing of slip through the San Gorgonio Pass. Airborne LiDAR from the B4 dataset was used to identify and measure preserved scarps that cut the terrace surfaces. The northernmost fault (F1) with an observed northward dip of 45 degrees vertically offsets units Qf2 and Qf3 by 1.4 ± 0.7 m and 2.9 ± 0.5 m respectively. The southern fault (F2), a 30 degree north dipping active oblique strike-slip thrust fault, vertically offsets units Qf1 and Qf4 by 1.5 ± 0.6 m, and 12.7 ± 1.4 m respectively. Geomorphic evidence suggests a roughly 3:1 lateral to vertical slip relationship, and with this we mathematically resolve these vertical slip parameters onto their respective fault plane geometries to evaluate the strike-slip component of motion. The strike-slip component, in conjunction with the age constraints gives the following Holocene strike-slip rates: northern fault (F1): 1.6 ± 1.1 mm/yr; southern fault (F2): 5.4 ± 1.1 mm/yr. Summation of these rates across the study area yields 7.0 ± 2.2 mm/yr for the Holocene strike-slip rate through the San Gorgonio Pass. These faults, suspected of carrying the majority of San Andreas motion through the SGP, are interpreted to release interseismic strain during large magnitude earthquakes of Mw 7 or greater (Yule and Sieh, 2003).

Using B4 LiDAR and CRN age data to constrain slip rates along the San Andreas Fault System at Millard Canyon, San Gorgonio Pass

Desjarlais, Ian C., Yule, J.D., Heermance, R.V.

Background

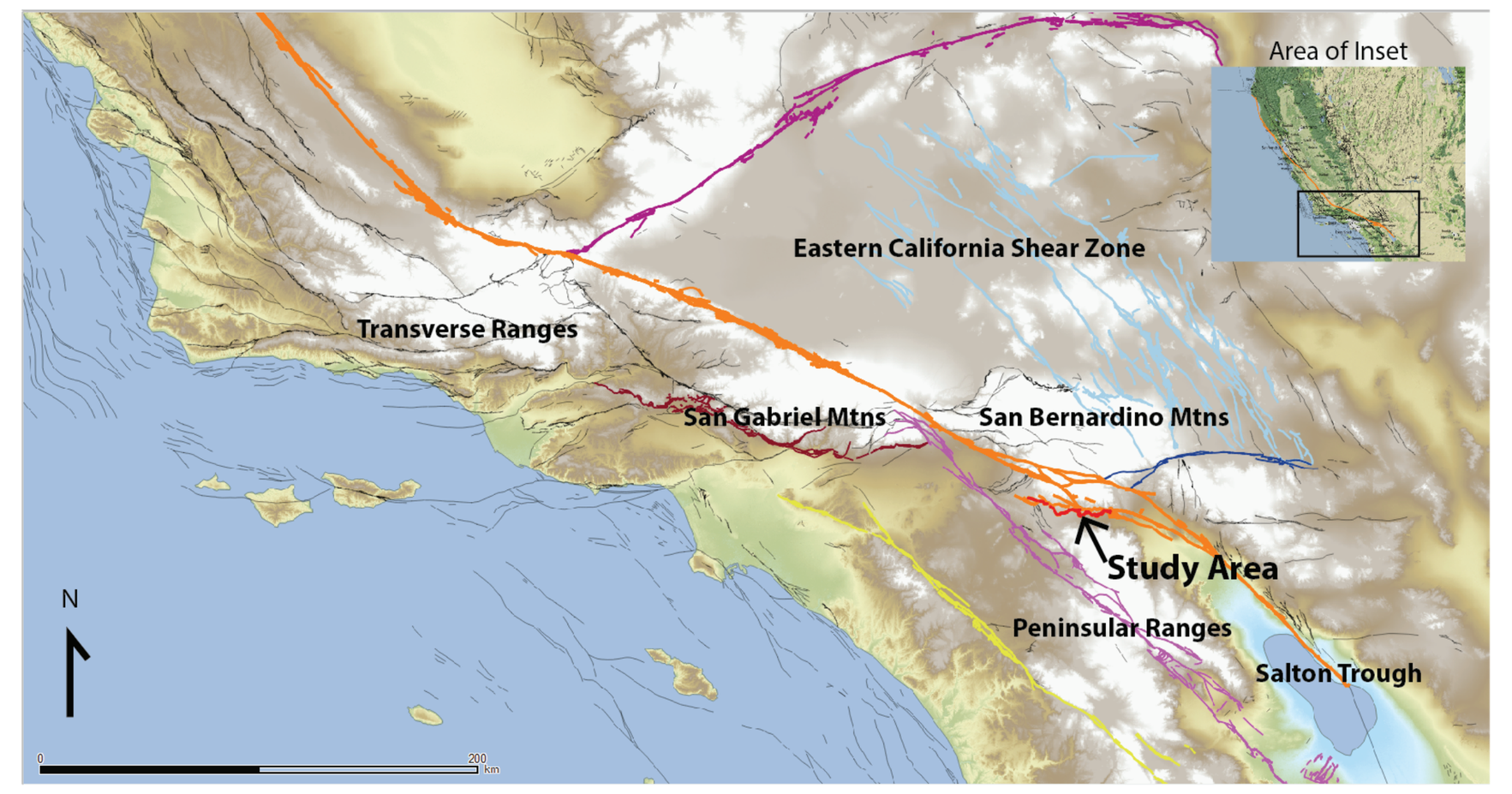

Southern San Andreas Fault Zone (SSAFZ) and secondary fault zones capable of large magnitude rupture. Fault name is followed by: color and probable magnitude of next event (Jennings 1994; Petersen and Wesnousky 1994; Jones 1995; Wesnousky 1986). Elsinore Fault (Yellow)/Mw 6.5-7.5; San Jacinto Fault (Magenta)/ Mw 6.5-7.5; Pinto Mountain Fault (Dark Blue)/ Mw 6.5-7.5; Sierra Madre Fault (maroon)/ Mw 6.0-7.0; Garlock Fault (Purple)/ Mw 6.8-7.6; Eastern California Shear Zone (Light Blue)/Mw 6.0-7.4; San Andreas Fault Zone (Orange)/ Mw 7.8+. San Gorgonio Pass Fault highlighted in red, arrow shows location of study area.

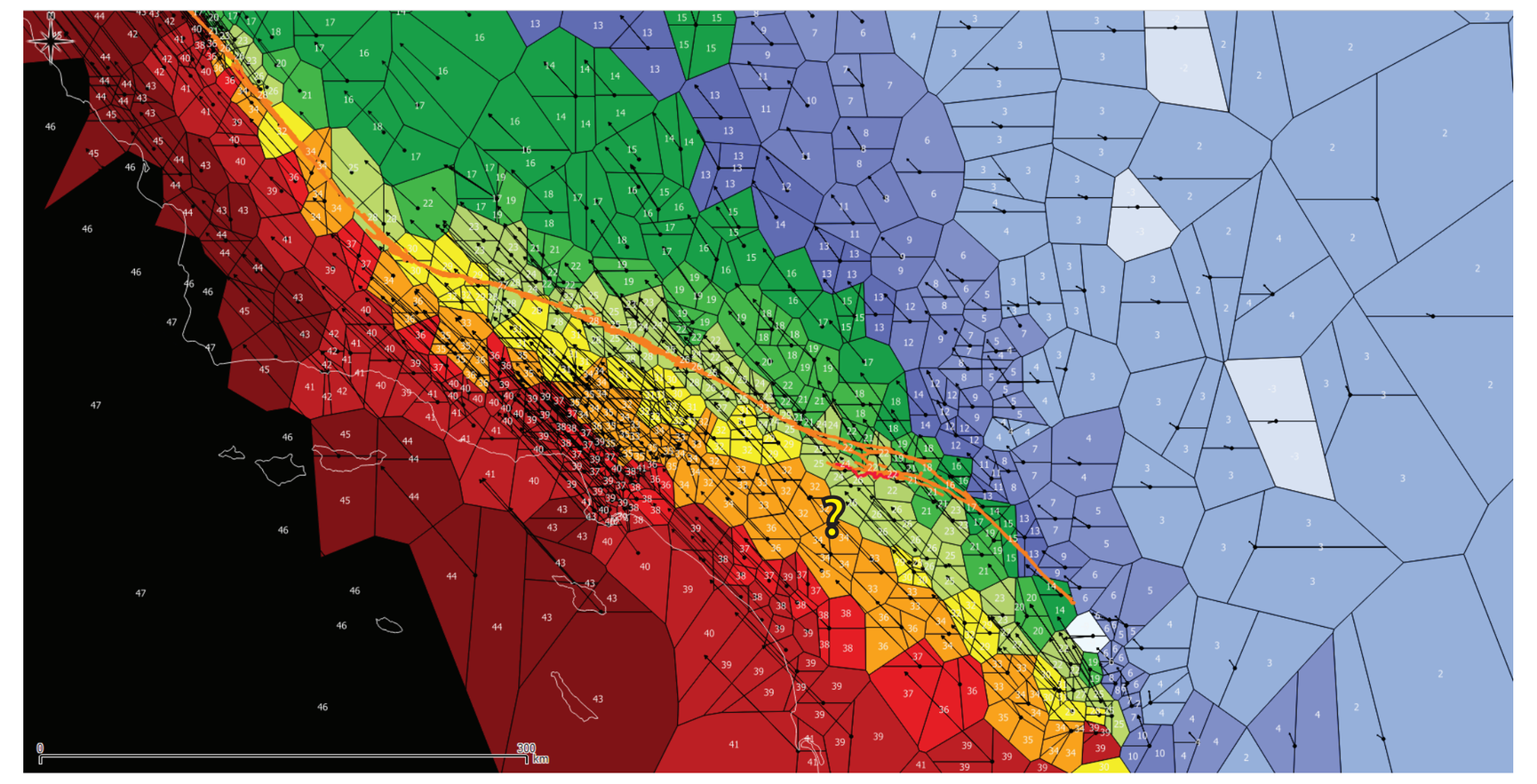

Regional map of southern California showing voronoi polygon analysis for geodetic stations and graduated crustal velocity field. Cross-over of pea-green velocity field (ā 24mm yr^{-1}) at the SGP, and absence of yellow (ā 30.5mm yr^{-1}) velocity field southwest of SGP indicates differential velocities across a major fault. These geodetic velocities are derived from relatively instantaneous data range (compared to earthquake recurrence interval (RI) of 500 yrs or more) and so do not represent motion resulting from long term cumulative coseismic deformation. The absence of the yellow velocity field southwest of SGP is therefore the result of the annual velocity defecit of the Penin-sular Range block (presumably due to complexities of SGP stepover). Geodetic velocity data from UNAVCO.

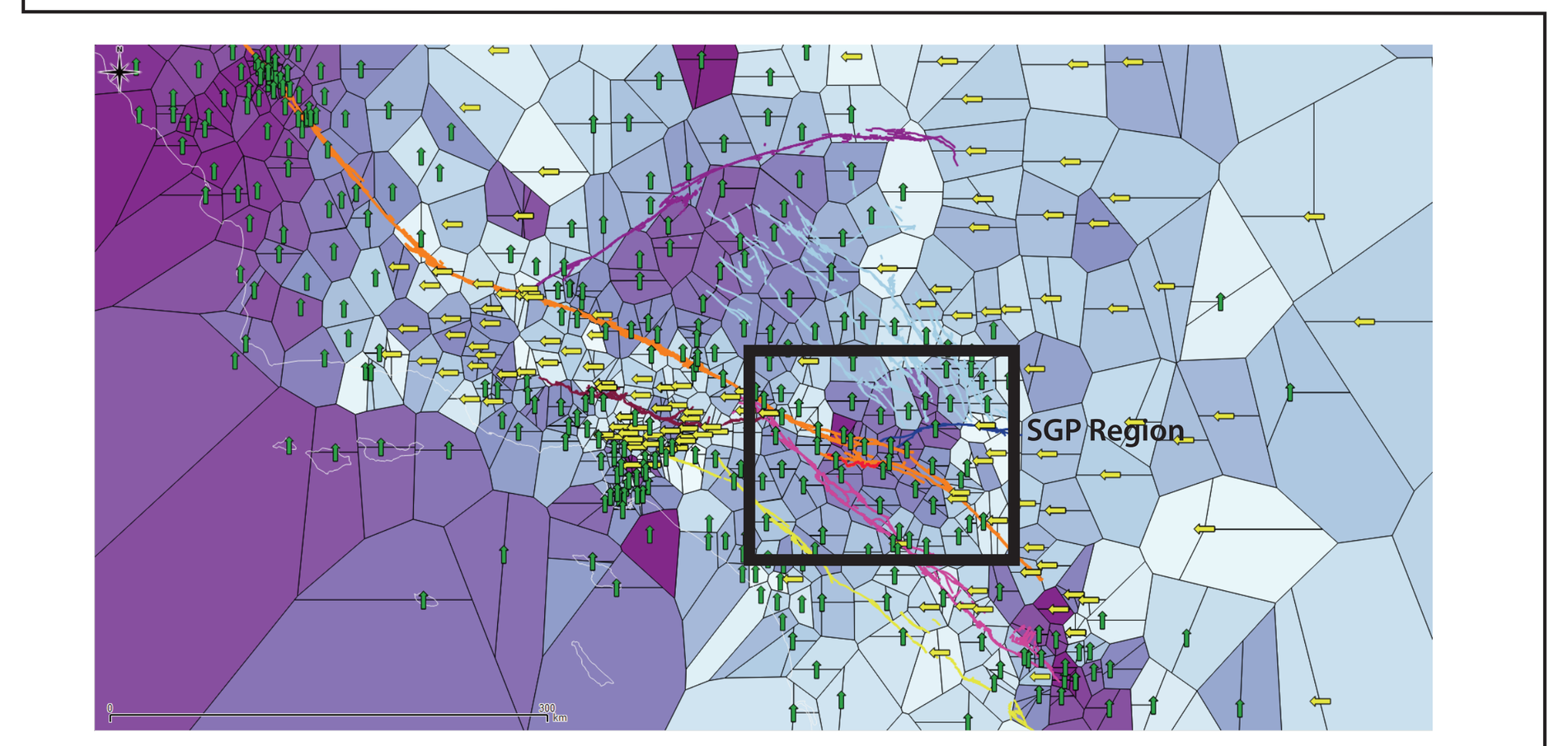

Analysis of southern California geodetic crustal velocities using voronoi polygons. Northing and easting components of motion are parsed from geodetic data and evaluated. Green arrows represent stations with greater northing components, yellow arrows represent stations with greater easting (westing) components. Darkness of voronoi color ramp indicates magnitude of differential between two components (i.e. darker purple indicates greater difference). This analysis is useful to visualize possible rotational and "torsional" behaviours of geodetic station domains and illustrates the complex forces responsible for southern California seismicity. Note cluster of darker polygons at center of San Gorgonio Pass region (in box). Dark cluster to northwest of black box is coincident with Garlock fault; stonger northing velocity component is result of left lateral strike slip. Boundaries of voronoi polygons are perpen-dicular lines at equidistant location between two adjacent geodetic stations (seeds). Geodetic velocity data from UNAVCO.

Abstract

Fault scarps cut a series of Holocene alluvial fan surfaces in Millard Canyon, within the San Gorgonio Pass (SGP). These fault scarps are likely the result of coseismic slip along the San Andreas Fault system during potentially large magnitude (Mw7+) earthquakes. Here we provide new ages for Holocene surfaces Qf2, Qf3, and Qf4. Charcoal fragments beneath Qf2 limits the surface to 1270 ± 80 years before present (ybp) and new 10Be exposure ages from the two older Holocene surfaces provide age constraints of 4800 ± 1600 ybp for Qf3 and 6800 ± 550 ybp for Qf4. These new ages provide limits on the timing of slip through the San Gorgonio Pass. Airborne LiDAR from the B4 dataset was used to identify and measure preserved scarps that cut the terrace surfaces. The northernmost fault (F1) with an observed northward dip of 45° vertically offsets units Qf2 and Qf3 by 1.4 ± 0.7m and 3.1± 0.7m respectively. The southern fault (F2), a 30° north dipping active oblique strike slip thrust fault, vertically offsets units Qf1 and Qf4 by 1.5 ± 0.6m, and 12.7 ± 1.4m respectively. We then mathematically resolve these vertical slip parameters onto their respective fault plane geometries to evaluate the strike slip component of motion along the N45W slip vector of the San Andreas Fault. The strike slip component, in conjunction with the age constraints gives the following Holocene strike slip rates: northern fault (F1): 1.8 ± 0.7 mm/yr; southern fault (F2): 8.8 ± 1.6 mm/yr. Summation of these rates across the study area yields 10.6 ± 2.3 mm/yr for the Holocene strike slip rate through the San Gorgonio Pass. These faults, suspected of carrying the majority of San Andreas motion through the SGP are interpreted to release interseismic strain during large magnitude earthquakes of Mw 7 or greater (Yule and Sieh, JGR 2003).

Methods

Field mapping based off previous work (Yule and Sieh, 2003) was performed to spatially characterize alluvial bodies and terrace riser relationships. Using QGIS 2.6 Brighton and QT Modeler Software suite, we quantitatively evaluate B4 LiDAR data to study the geomorphology of Millard Canyon and its periphery. Using GDAL and GRASS we derive point cloud slope and contour rasters to locate ideal cross section locations. Scarp profiles are generated perpendicular to slope contours and scarp trends. Vertical uplift is determined by measuring Z-component of scarp profiles (See Profiles A,B,C,D this poster). This component can then be resolved along a plane equivalent to the established dip of the fault. We process and analyze samples for cosmogenic ^{10}Be and determine nuclide ratios with the Accelerator Mass Spectrometer at Lawrence Livermore National Lab (LLNL). Surface age divided by slip yields deformation rate. Boundaries of voronoi polygons are perpendicular lines at equidistant location between two adjacent geodetic stations (seeds). In absence of an infinite and homogenous array of geodetic stations (ideal), voronoi polygons represent best-known lateral extent of station domain.

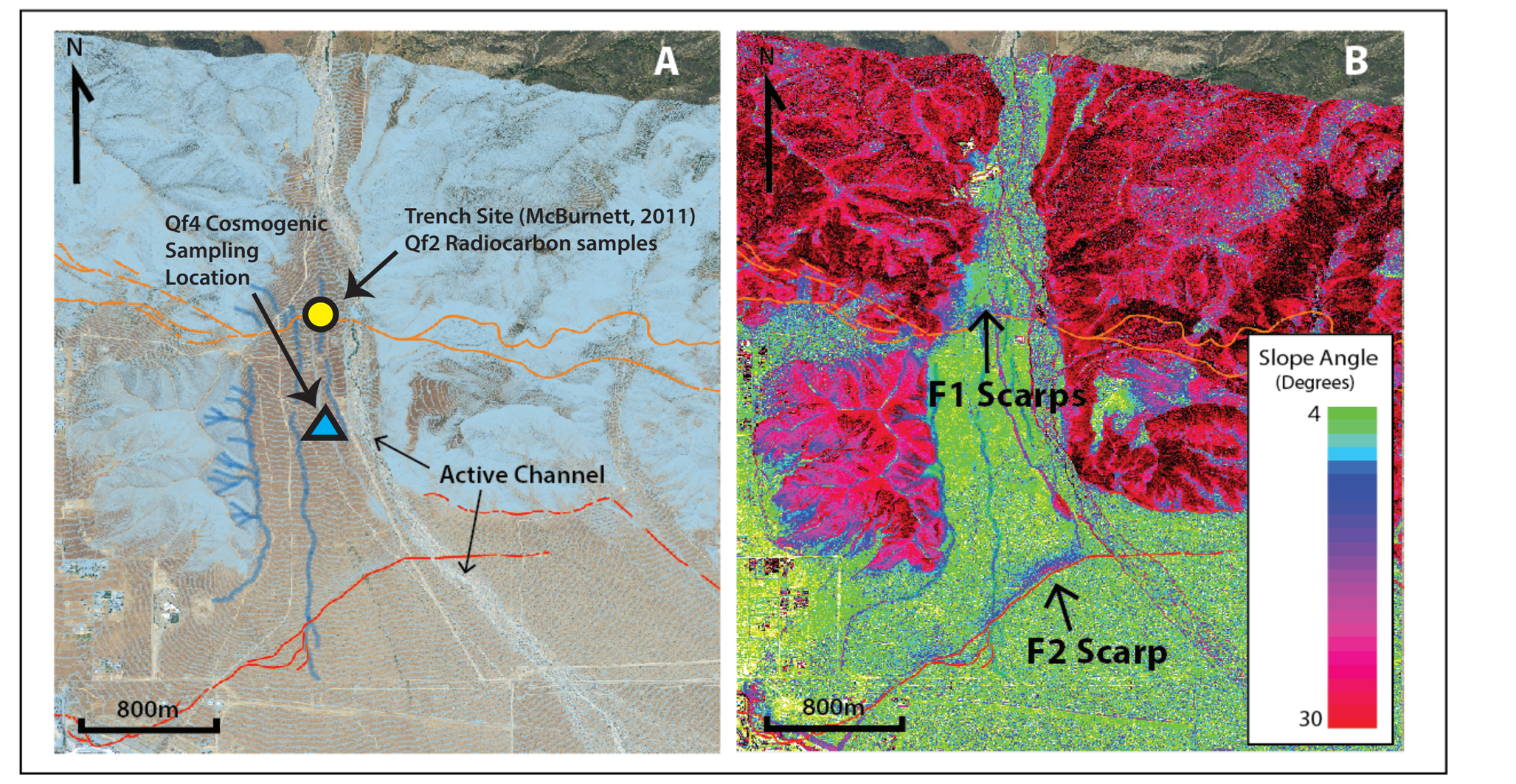

A. High resolution 0.5m contour interval map derived from B4 LiDAR dataset, extracted with GDAL v.1.2.29 using QGIS Brighton v.2.6. Surface runoff rivulets traced in blue are mapped using contours and USGS orthorectified aerial imagery. Northeasternmost rivulet is a result of well pump test discharge during groundwater production well installation. Fault F1 in orange, fault F2 in red. Triangle shows locations of Qf4 cosmogenic samples; circle shows location of radiocarbon samples from trench site of Mcburnett (2011). B. High resolution slope map derived from B4 LiDAR dataset, generated using GRASS 6.4.3 raster processing module. Warmer colors represent steeper slope and is used to delineate scarp fronts from base level surfaces, and to determine ideal cross section locations.

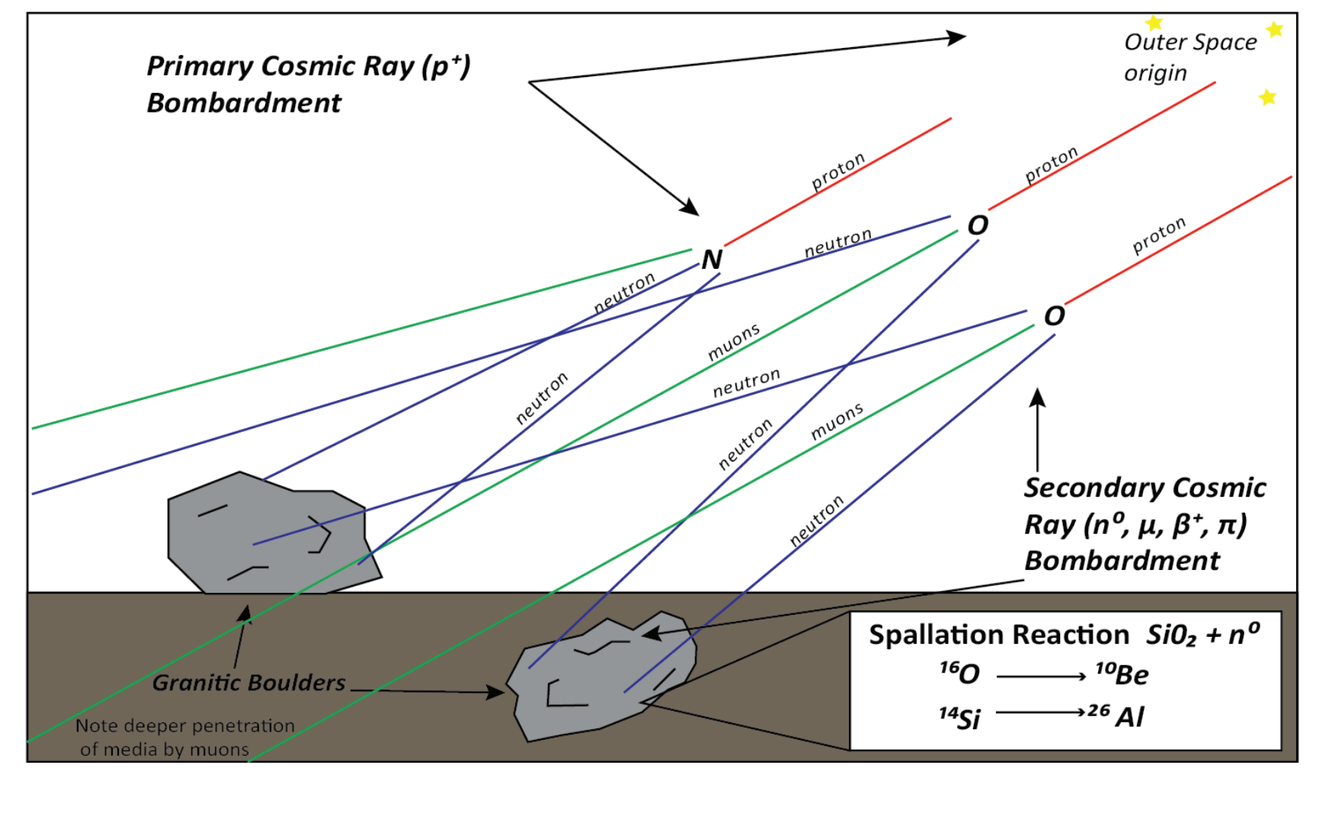

Formation of in-situ Cosmogenic Radionuclides (CRN) by spallation reactions. Primary cosmogenic rays originate in outer space from many sources including supernovae. Nucleons (primarily protons) bombard atmospheric gases such as Nitrogen (N) and Oxygen(O), releasing secondary cosmic rays as neutrons (n^0), muons (μ), positron(β+) and pions (π). Neutrons and muons which play the largest role in CRN production, advance towards the earth surface impacting quartz (SiO_2) containing materials such as granite and siliciclastic alluvium (Lal, 1991). The impact causes spallation fission reactions to occur forming ^{10}Be and ^{26}Al isotopes from ^{16}O and ^{14}Si respectively. Neutron penetration diminishes with depth, with total attenuation at depths greater than ~3m (Gosse, 2012). Muons may penetrate much deeper than neutrons especially in low density rock media such as alluvium, and can effectively form CRNs up to depths of 30m at very low production rates.

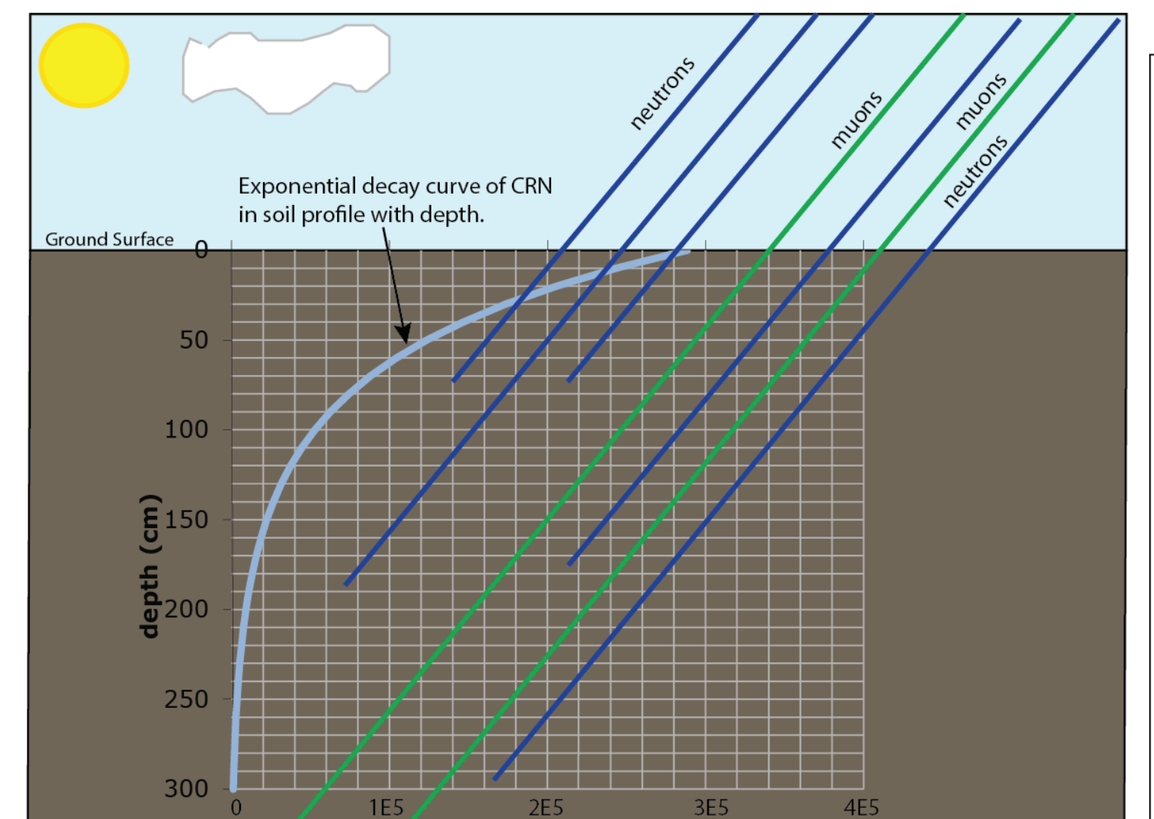

Depth Profile Concept. Incoming neutrons (blue) and muons (green) penetrate through the soil column causing spallation reactions to occur at depth. Neutrons can penetrate to depths of ~3m beneath surface; muons may penetrate down to 30m beneath surface. Attenuation of neutron penetration causes exponential decrease in production rate of CRN. This characteristic is the theoretical basis of depth profile method to determine CRN inheritance values. This figure shows soil with zero inheritance; CRN concentration curve approaches zero at roughly 3m depth.

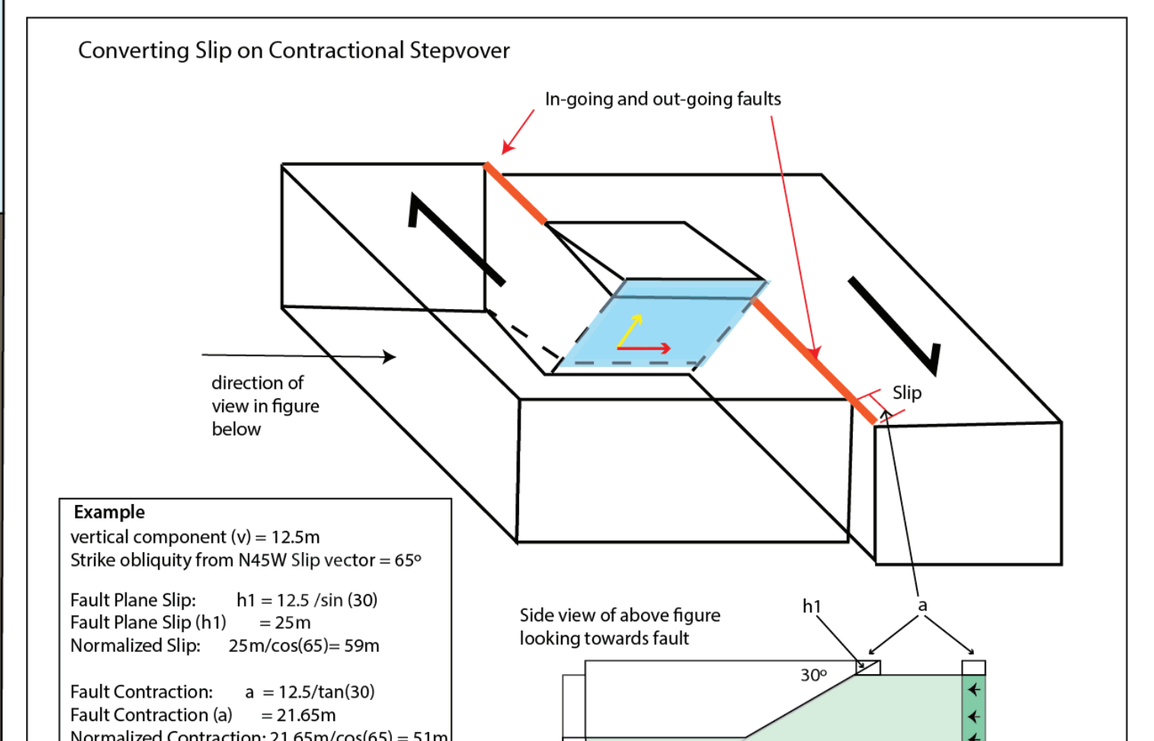

Dip-slip component (yellow vector) directly measures horizontal contraction, which is equivalent to slip(a) on the fault (in orange). This assumes an ideal 90º angle between stepover plane and main fault, however the structural complexities of the SGP stepover require similar yet alternate trigonometric resolution. We define 'slip' as the net movement on the fault plane (Sharp, 1975). Summed oblique slip vector is resolved onto the N45W slip vector of the San Andreas fault (see example at left). This gives SAF normalized slip rates. Modified from Figure 6B Spotila et al 1986.

Data

Cosmogenic Data

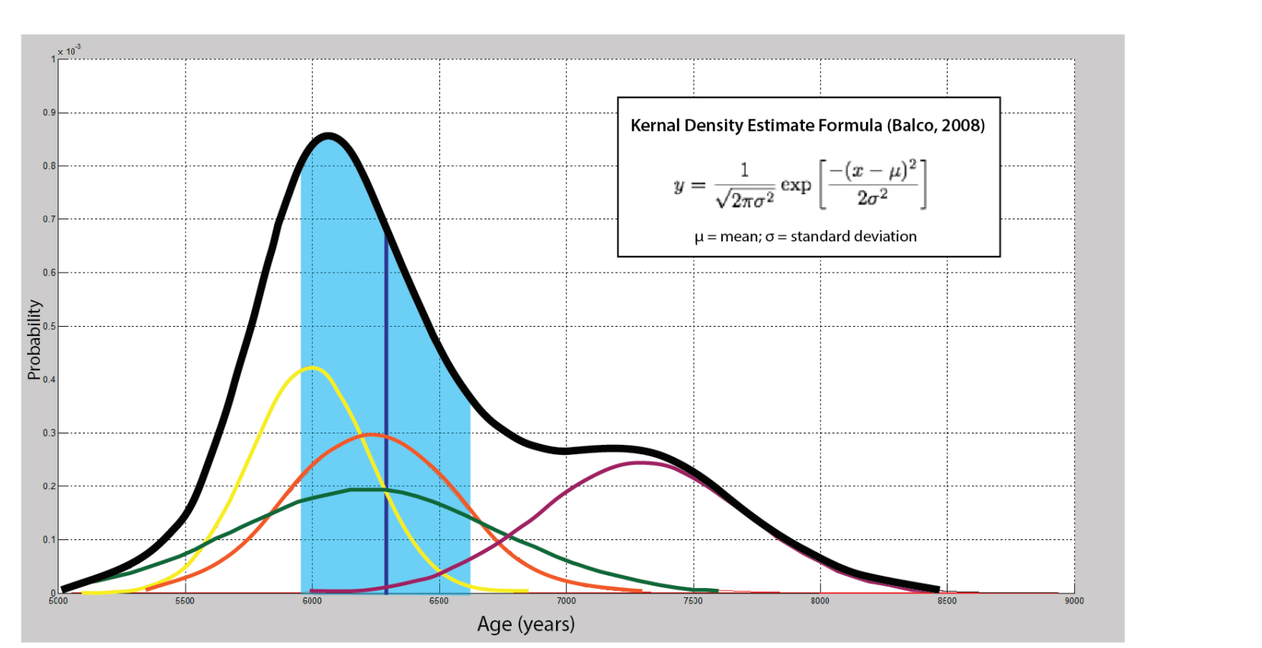

Camel Plot of Qf4 boulders. Curves represent smoothed frequency distribution of age data. Frequency overlap yields synergistic summation of probability thereby indicating the most probable age for the surface based on error range of each sample. Most probable age is indicated by highest peak of the summed kernel density estimate (Balco, 2008). Model was run in Matlab 2014 using CamelPlot code of Balco (2008). Mean weighted average (WMA) age for the Qf4 boulder suite is 6285 ± 330 years, overlain in blue (ISOPLOT 4) . We adopt the MWA for use in calculating age of Qf4 surface with Qf4 depth profile. Sample 1303-B1 (green); 1303-B2 (magenta); 1303-B3 (orange); 1303-B4 (yellow).

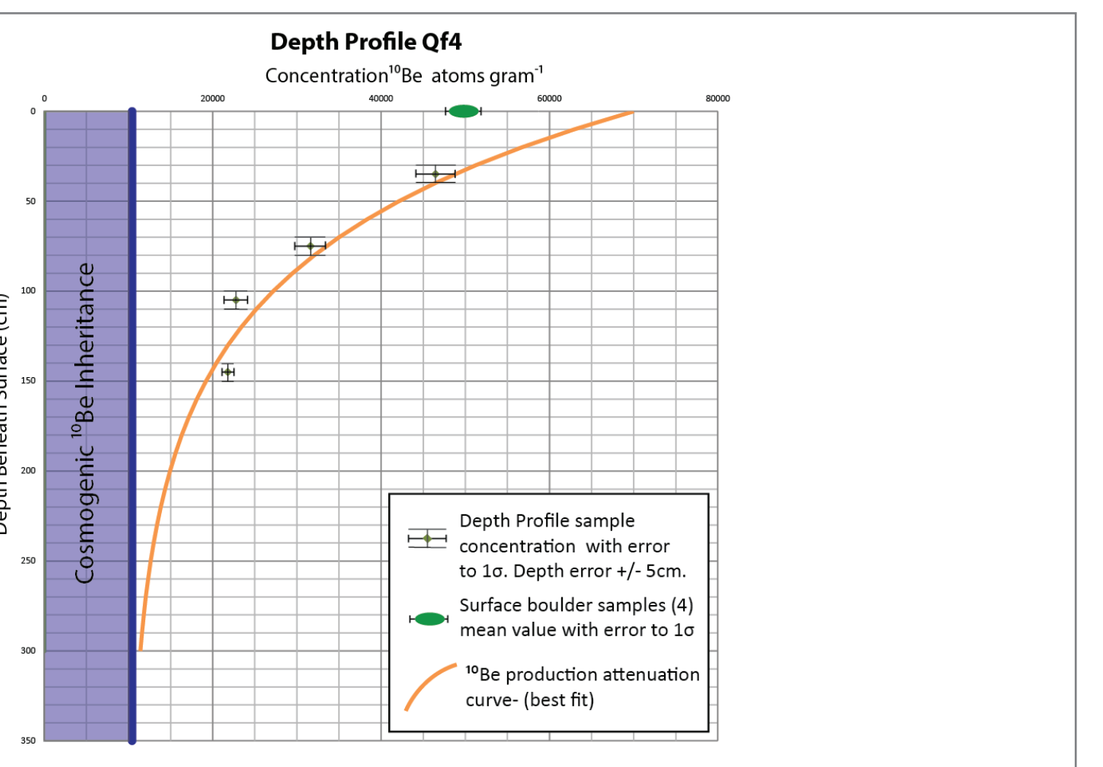

Depth profile curve for Qf4 alluvium of Millard Canyon, San Gorgonio Pass. Samples plotted alongside CRN production decay curve. Data indicates ~10k atoms g^{-1} nuclide inheritance in samples, similar to measurments obtained from the active channel. Sample ^{10}Be concentrations plotted with 1-sigma error. Sample depth plotted with 5cm error. Linear regression of sample concentrations gives age of 776 ± 979 years

Geochronolgy of Millard Canyon Surfaces

All ages in calibrated years before present (ybp).

Surface	^{14}C	^{10}Be	Notes
Qf1	890 ± 300		Age constrained between Qf0 and Qf2. No direct dating.
Qf2	1270 ± 80		Charcoal sample beneath Qf2 surface (McBurnett, 2011).
Qf3		4800 ± 1600	Age constrained between Qf2 and Qf4. No direct dating.
Qf4		6800 ± 550	^{10}Be Depth profile + 4 surface boulders.

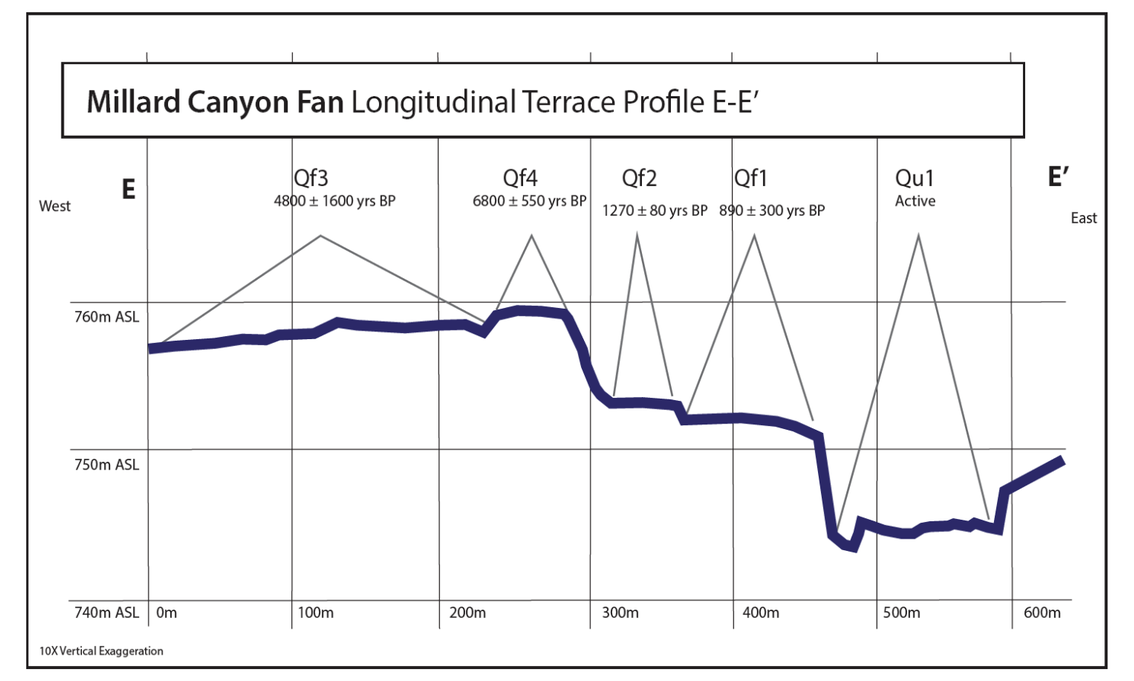

Millard Canyon alluvial fan terrace cross-sectional profile. Figure shows surface ages for abandoned surfaces of erosional terraces. Profile obtained from B4 LiDAR dataset using QT Modeler software suite version 8.02. 10x Vertical exaggeration. See Tectonic Geologic Map (below, left) for location.

LiDAR Cross Sections

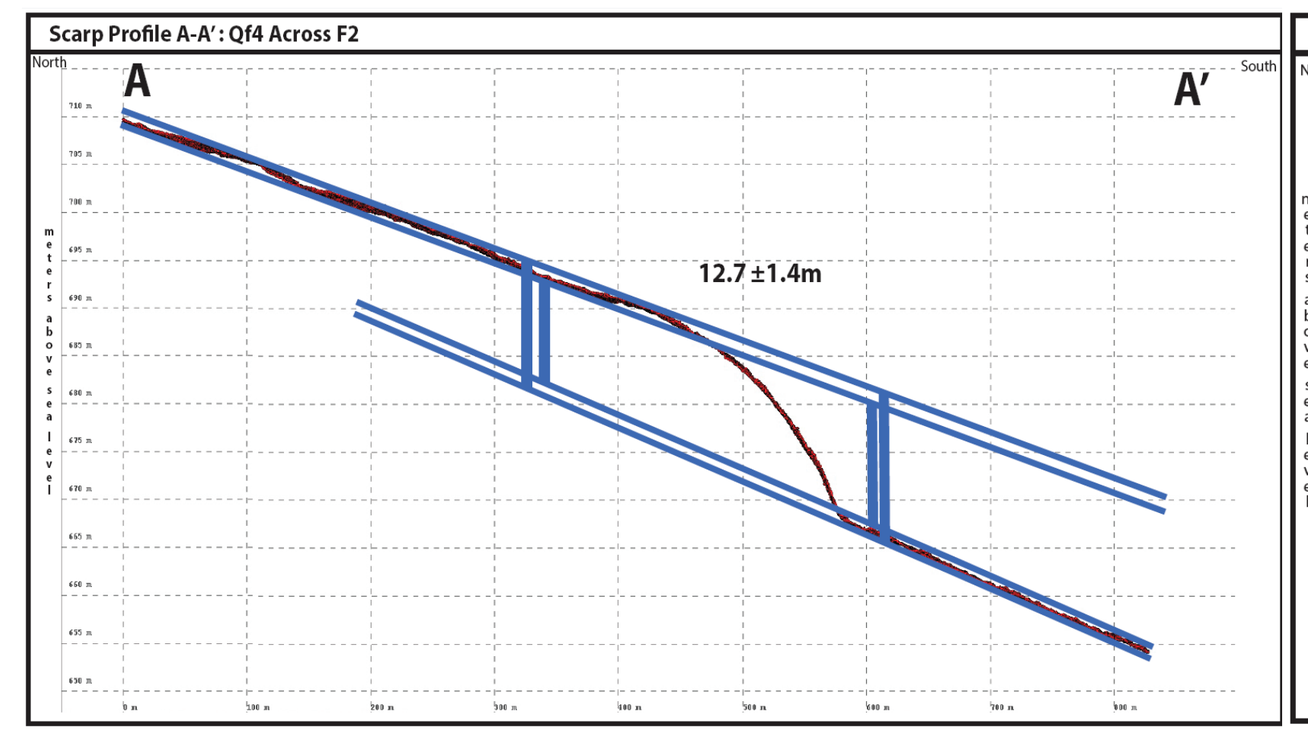

Fault F2 (southern) scarp, cross-sectional profile. Scarp preserves approximately 12.7 ± 1.4 meters vertical displacement of Qf4 surface. Profile obtained from B4 LiDAR dataset using QT Modeler software suite version 8.02. Cross section swath width set to 10m. Point cloud density = 2.98 points/m².

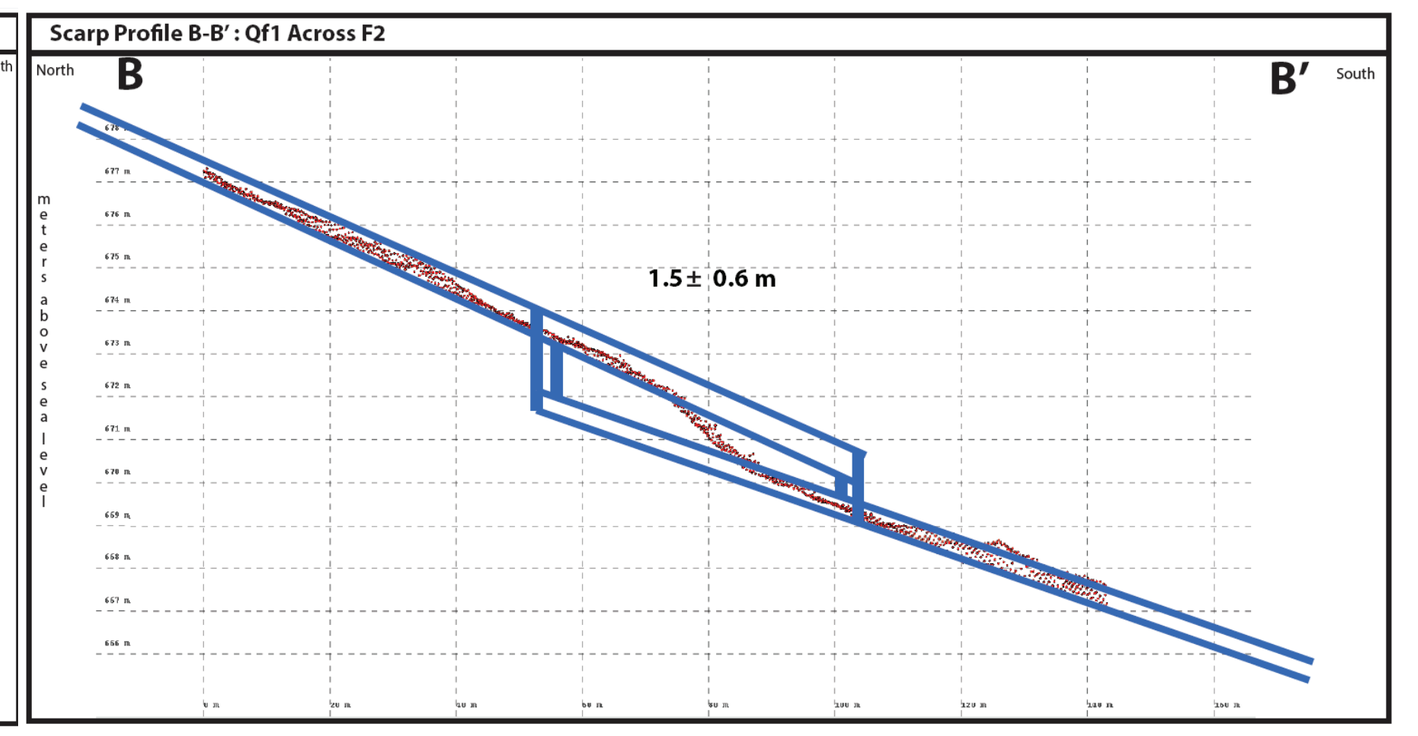

Fault F2 (upper) scarp, cross-sectional profile. Scarp preserves approximately 1.5 ± 0.6 meters vertical displacement of Qf1 surface. Profile obtained from B4 LiDAR dataset using QT Modeler software suite version 8.02. Cross section swath width set to 2 meters. Point cloud density = 2.98 points/m².

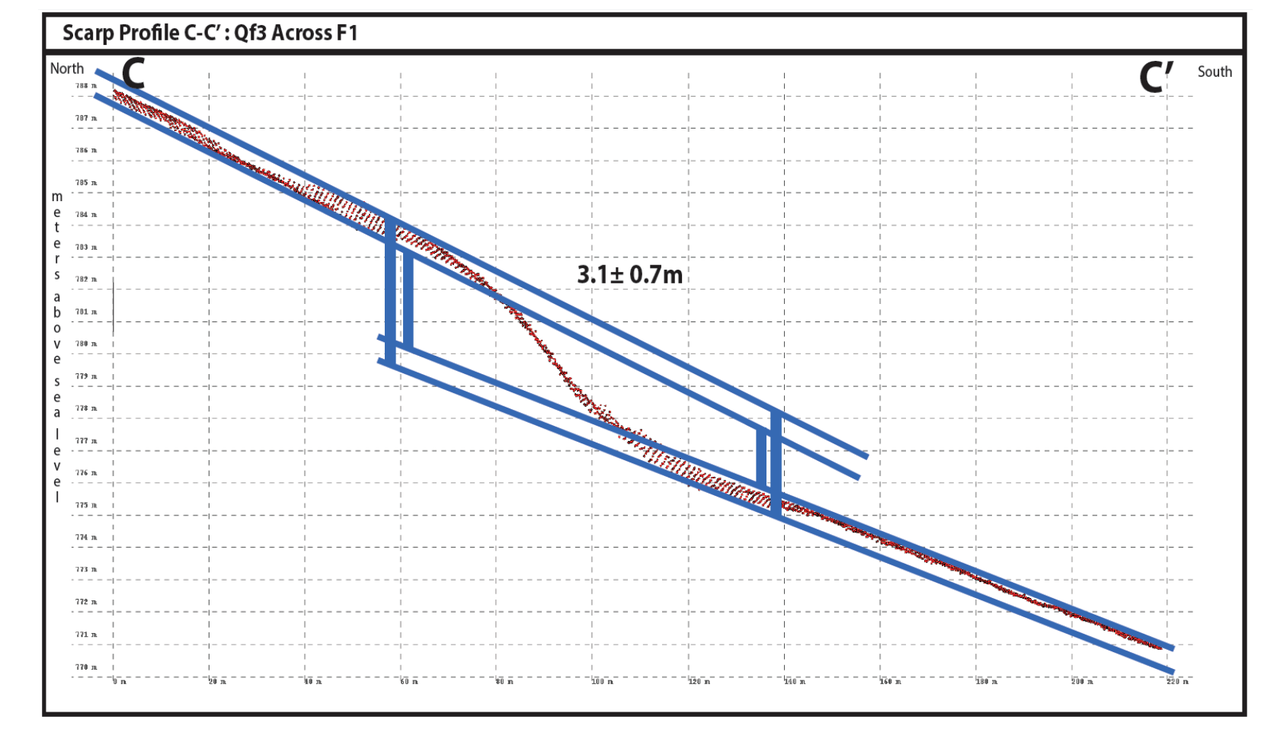

Fault F1 (upper) scarp, cross-sectional profile. Scarp preserves approximately3.1 ± 0.7 meters vertical displacement of Qf3 surface. Profile obtained from B4 LiDAR dataset using QT Modeler software suite version 8.02. Cross section swath widthset to 3 meters. Point cloud density = 2.98 points/m².

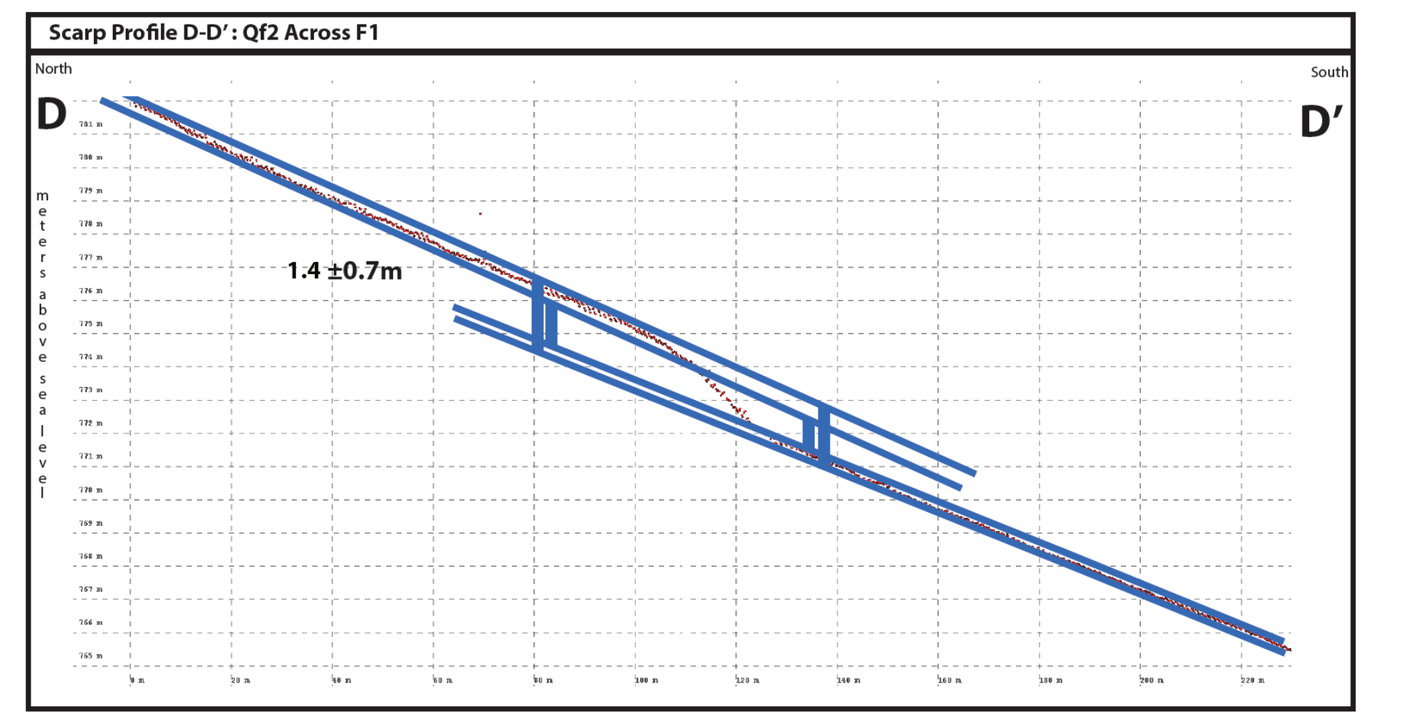

Fault F1 (upper) scarp, cross-sectional profile. Scarp preserves approximately 1.4 ± 0.7 meters vertical displacement of Qf2 surface. Profile obtained from B4 LiDAR dataset using QT Modeler software suite version 8.02. Cross section swath width set to 3 meters. Point cloud density = 2.98 points/m².

Tectonic Geologic Map

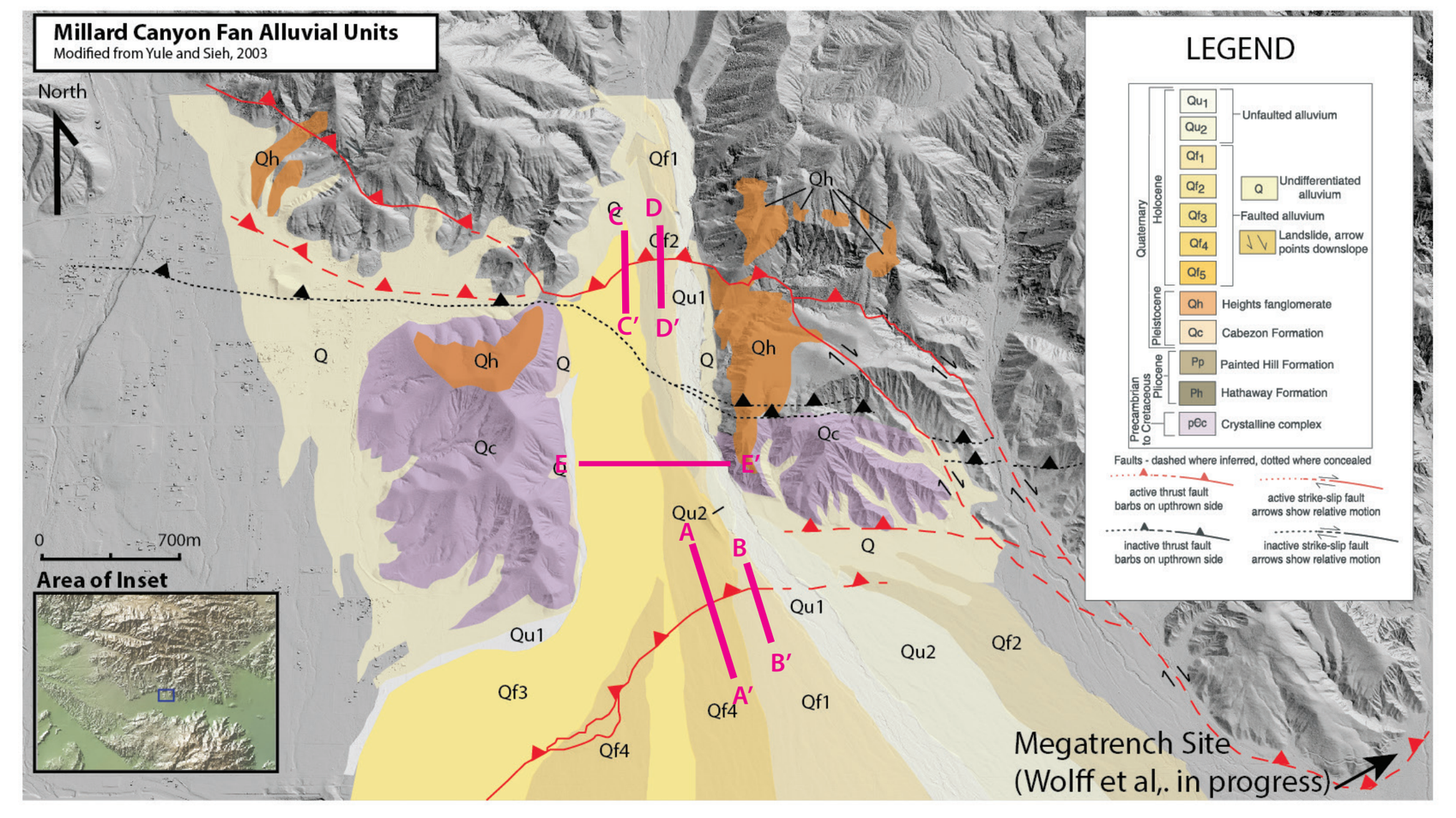

Tectonic geologic map of Millard Canyon showing alluvial fan units based off of Yule and Sieh, 2003. Map units include unfaulted alluvium (Qu1,Qu2) of the active channel. Older alluvium units Qf4,Qf3,Qf2,Qf1, record slip events as preserved scarps and are the focus of this study. Magenta lines represent location of LiDAR cross sections used in this study. Cross sections A- D show scarp perpendicular transects. Cross section E shows longitudinal terrace profile. See figures above in "Data" section.

Results

Vertical Displacement Rates and Paleoseismology

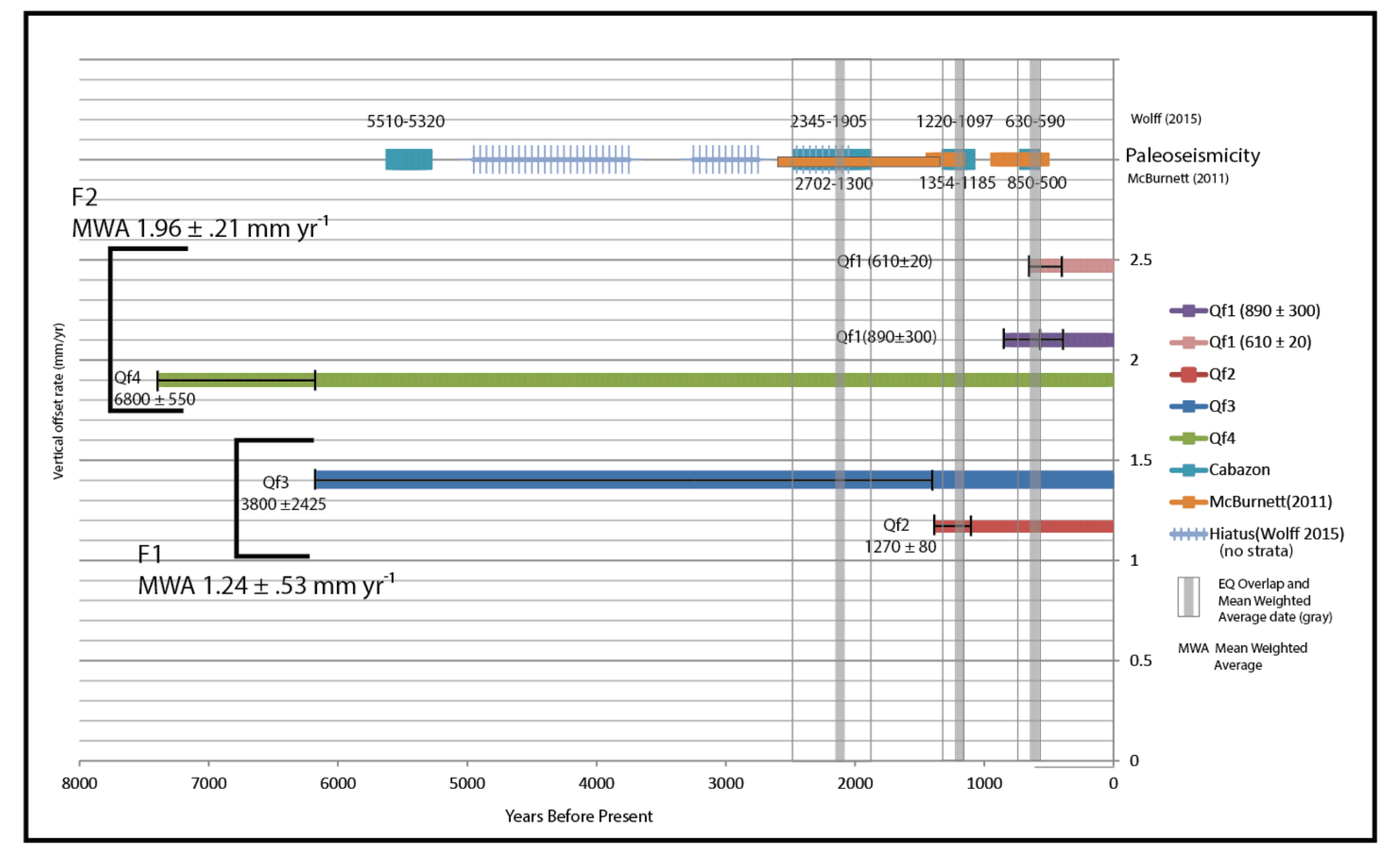

Plot showing vertical displacement rates (uplift) determined by offset of each Holocene alluvial surface in Millard Canyon. The bimodal character of the data grouping reinforces the interpretation of the independant fault behavior. Fault F1, offsetting Qf3 and Qf2 produces a mean weighted average vertical displacement rate of 1.24 ± 0.53 mm yr^{-1}. Fault F2 has a mean weighted average vertical displacement rate of 1.96 ± 0.21 mm yr^{-1}. Paleoseismic record of SGP determined by McBurnett (2011) and Wolff (In progress) depicted along top axis, showing possible contemporaneous surface abandonment and seismicity. This suggests abandonment of alluvial surfaces in Millard canyon to be driven by uplift.

San Andreas Slip Vector (N45W) Normalized Slip Rates

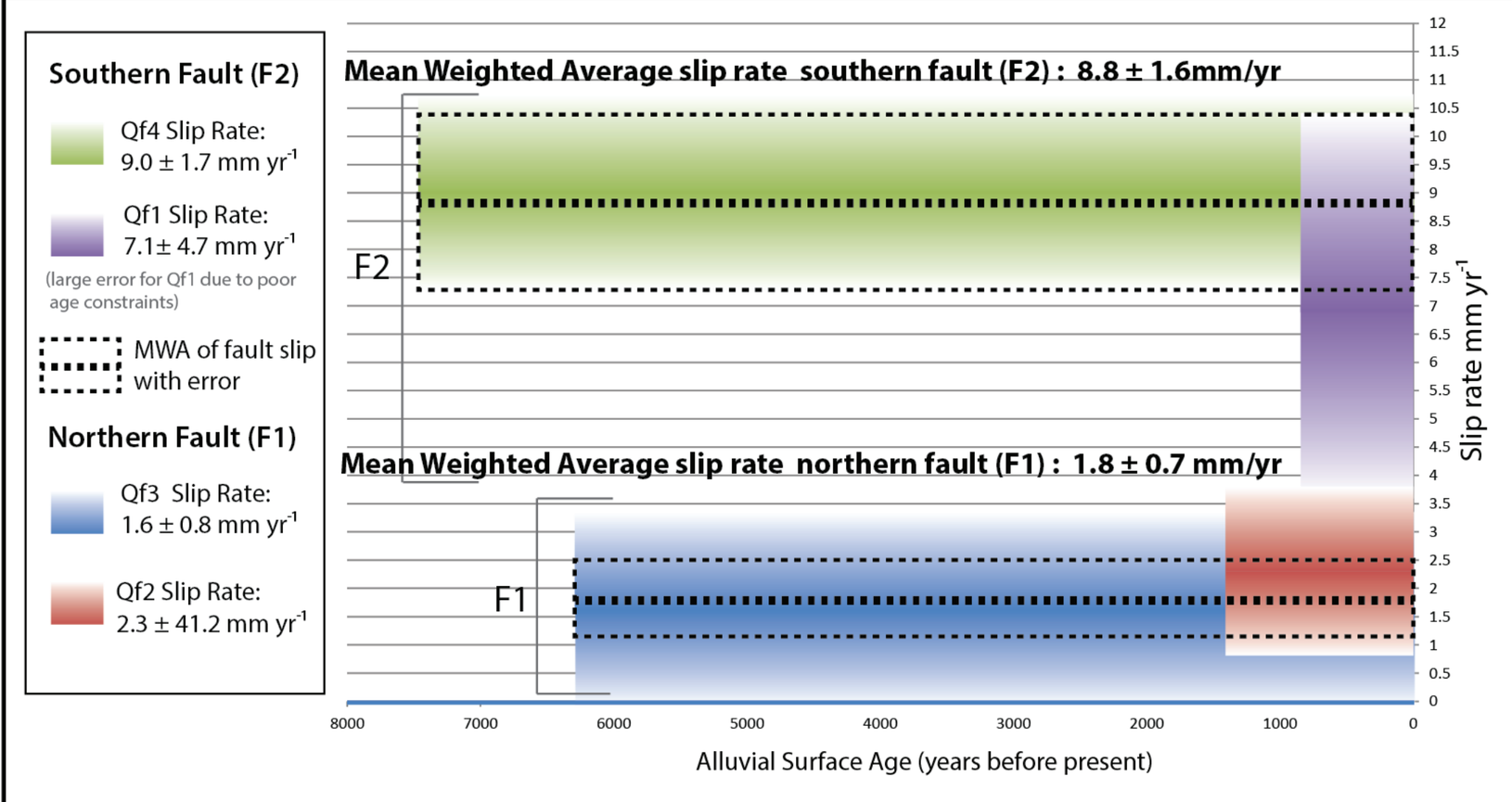

San Andreas Fault normalized slip rates from San Gorgonio Pass with 2σ error (represented as color ramp). We resolve slip vectors from Millard Canyon fault planes onto the N45W slip vector of the San Andreas Fault. We calculate the mean weighted average of the slip rates determined from each independant surface (F1: Qf3 & Qf2; F2: Qf4 & Qf1) to determine the preferred slip from each fault. Bimodal distribution of data reinforces characteristic slip behaviors of both northern and southern faults and partially validates our method of determining the slip rate with scarp heights and age constraints. The large error for Qf1 is the result of poor age constraint for the surface (890 ± 300 ybp). Results show the slip rate for F2 to be nearly 4 time greater than that of F1.

Kinematic Summary

	Age (ybp)	+/-	Fault Dip Angle (deg)	Obliquity (deg) from N45W	Vertical Displacement	+/-	Vertical Displacement Rate (mm yr-1)	+/-	Fault Plane Horizontal Contraction	+/-	N45W Horizontal Contraction	+/-	N45W Contraction Rate (mm yr-1)	+/-	Fault Plane Slip	+/-	San Andreas (N45W) Normalized Slip	+/-	SAF Normalized Slip Rate (mm yr-1)	+/-
Qf4 Cumulative			30	65	12.7	1.4	**1.9**	**0.4**	22.0	2.4	52.0	5.7	**7.8**	**1.5**	25.4	2.8	60.1	6.6	**9.0**	**1.7**
Qf4 Age	6800	550																		
Qf3 Cumulative			45	45	3.1	0.7	**0.8**	**0.4**	3.1	0.7	4.4	1.0	**1.1**	**0.6**	4.4	1.0	6.2	1.4	**1.6**	**0.8**
Qf3 Age	4800	1600																		
Qf2 Cumulative			45	45	1.4	0.7	**1.2**	**0.6**	1.4	0.7	2.0	1.0	**1.6**	**0.9**	2.0	1.0	2.8	1.4	**2.3**	**1.2**
Qf2 Age	1270	80																		
Qf1 Cumulative			25	65	1.5	0.6	**2.2**	**1.4**	3.2	1.3	7.6	3.0	**10.9**	**7.0**	3.5	1.4	8.4	3.4	**8.8**	**1.6**
Qf1 Age	890	300																		
F1 MWA(Holocene)							**1.2 ± 0.5**						**1.3 ± 0.5**						**1.8 ± 0.7**	
F2 MWA(Holocene)							**2.0 ± 0.2**						**7.9 ± 1.5**						**8.8 ± 1.6**	
F1+F2 Sum(Holocene)							**3.2 ± 0.7**						**9.2 ± 2.0**						**10.6 ± 2.3**	

Interpretation

Millard Canyon Tectonic Geomorphology

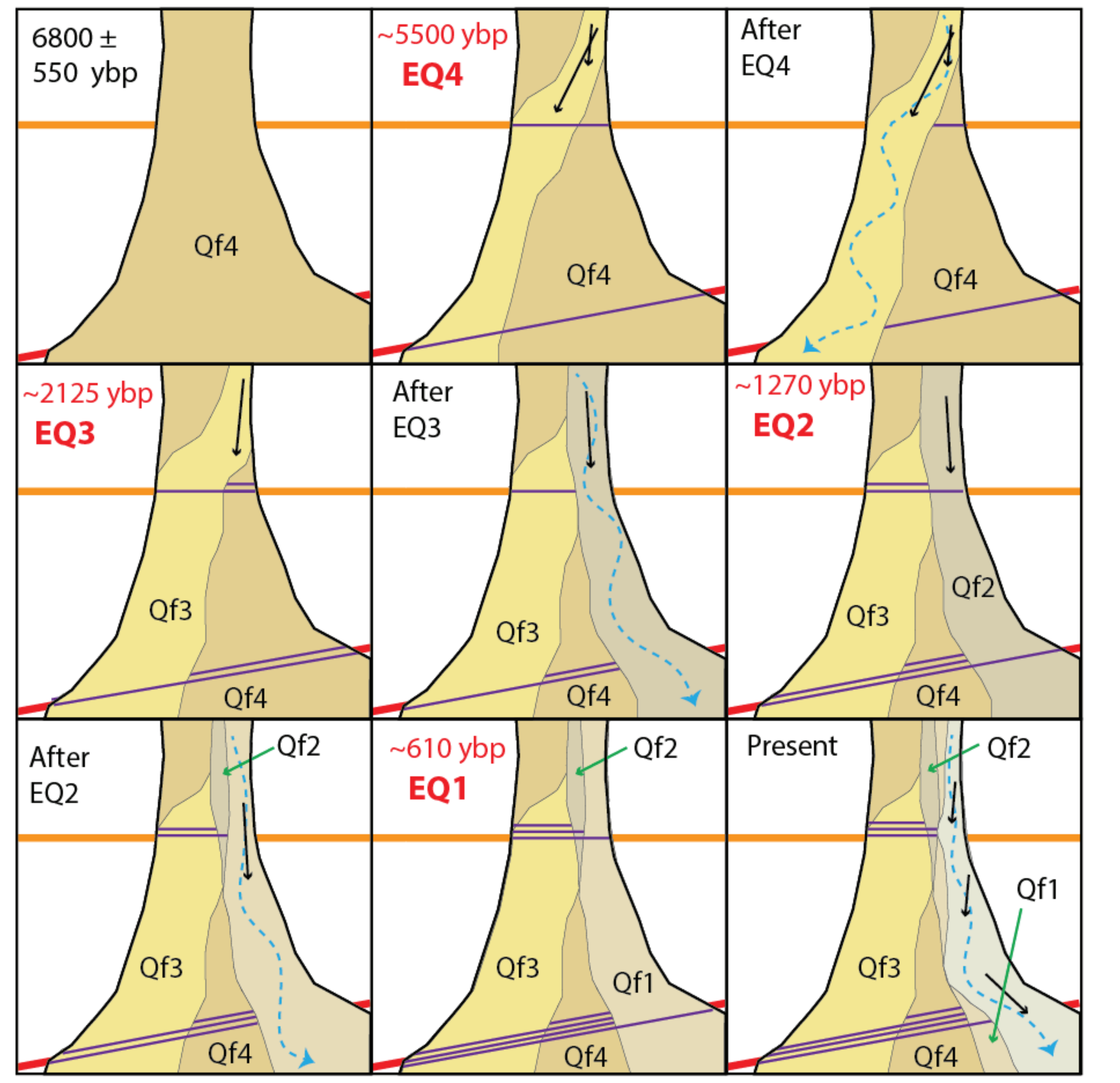

Schematic interpretation showing geomorphic evolution of Millard Canyon surfaces through time with cumulative imprint of (what may be an incomplete) paleoseismic record obtained from nearby trenching activities (McBurnett, 2011; Wolf et al., in progress). Model assumes contemporaneous rupture on northern and southern faults, however this behavior has not been proven to occur. Up to 2 seismic events may have occured between EQ4 and EQ3, but were not confirmed in this study. Ruptures represented as purple lines, showing known earthquakes 1-4. Disappearance of line illustrates erosion of scarp due to fluvial processes in active channel. Dashed blue line illustrates fluvial activity in channel. Black arrows illustrate suspected direction of hydrologic forces pertinant to fluvial geomorphology of channel. Text in red designates the time frame in which the earthquake occurred. Qf1, Qf2, Qf3, Qf4: faulted alluvium; Q: undifferentiated. See Figure 6 of Yule and Sieh, (2003) for detailed geologic map.

Implications

Uplift across the youngest scarps in Millard Canyon (cutting Qf1 and Qf2) records a minimum 5.5± 2.4m of localized slip during the most recent earthquake 590-630 yrs ago (Yule et al., this meeting). This amount of slip supports a model where elastic strain from SAFZ-linked crustal motion (N45W) accumulates across the SGPFZ at ~9.0± 2.0 mm/yr and is released by large, once-per-millennia earthquakes.

Significance

The partitioning of strain and slip along the complex network of faults within the southern San Andreas fault zone can be at-times responsible for obfuscating the observed relationship between geodetic and geologic rates of slip which are commonly in discordance. A growing body of collaborative data at key locations has aided in the shared goal of mitigating of this challenge. The objective of this study is to provide geologically-derived slip rates that will contribute to the community understanding of the slip partitioning through the structural knot of the San Gorgonio Pass Fault Zone.

Validation

A.

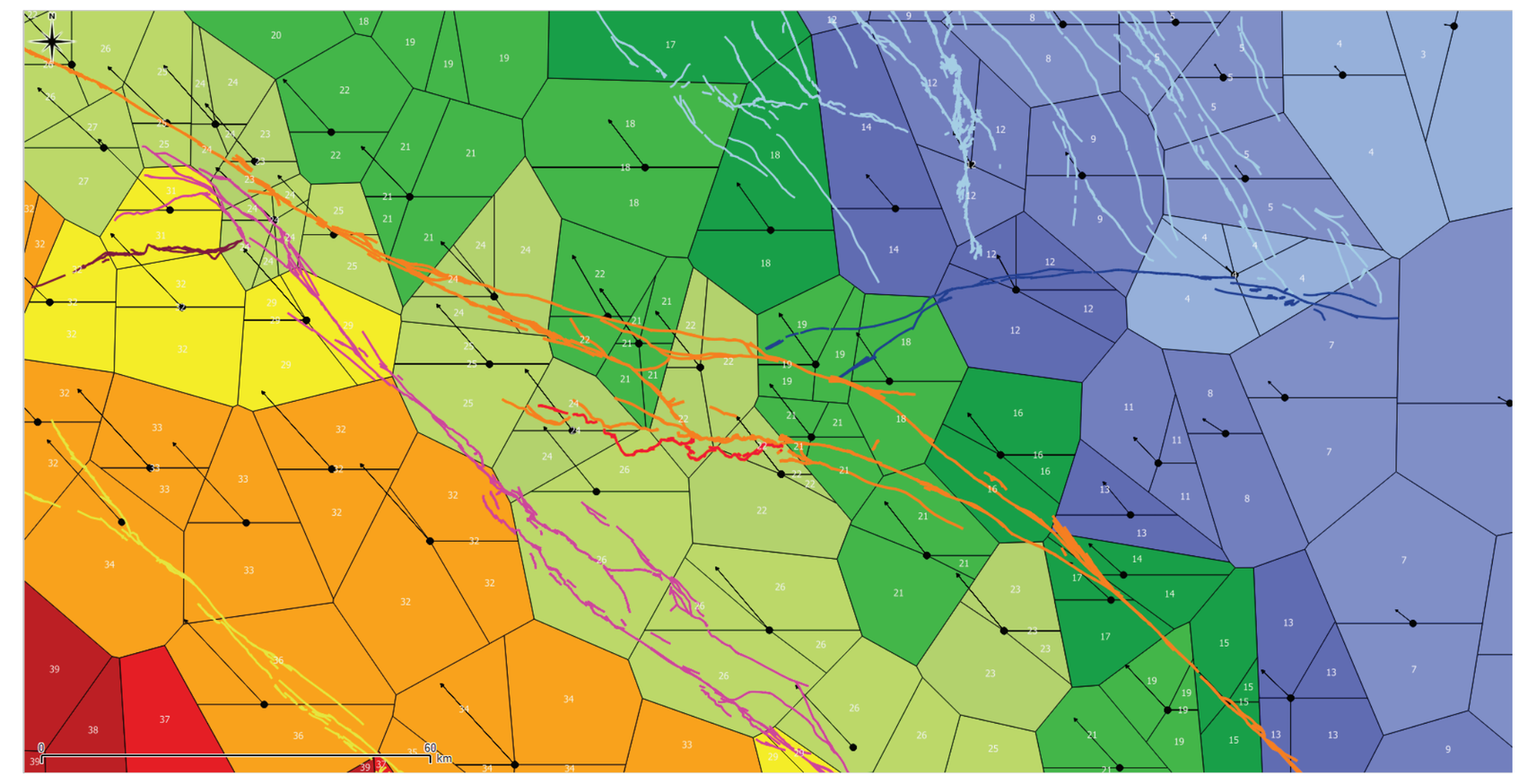

B.

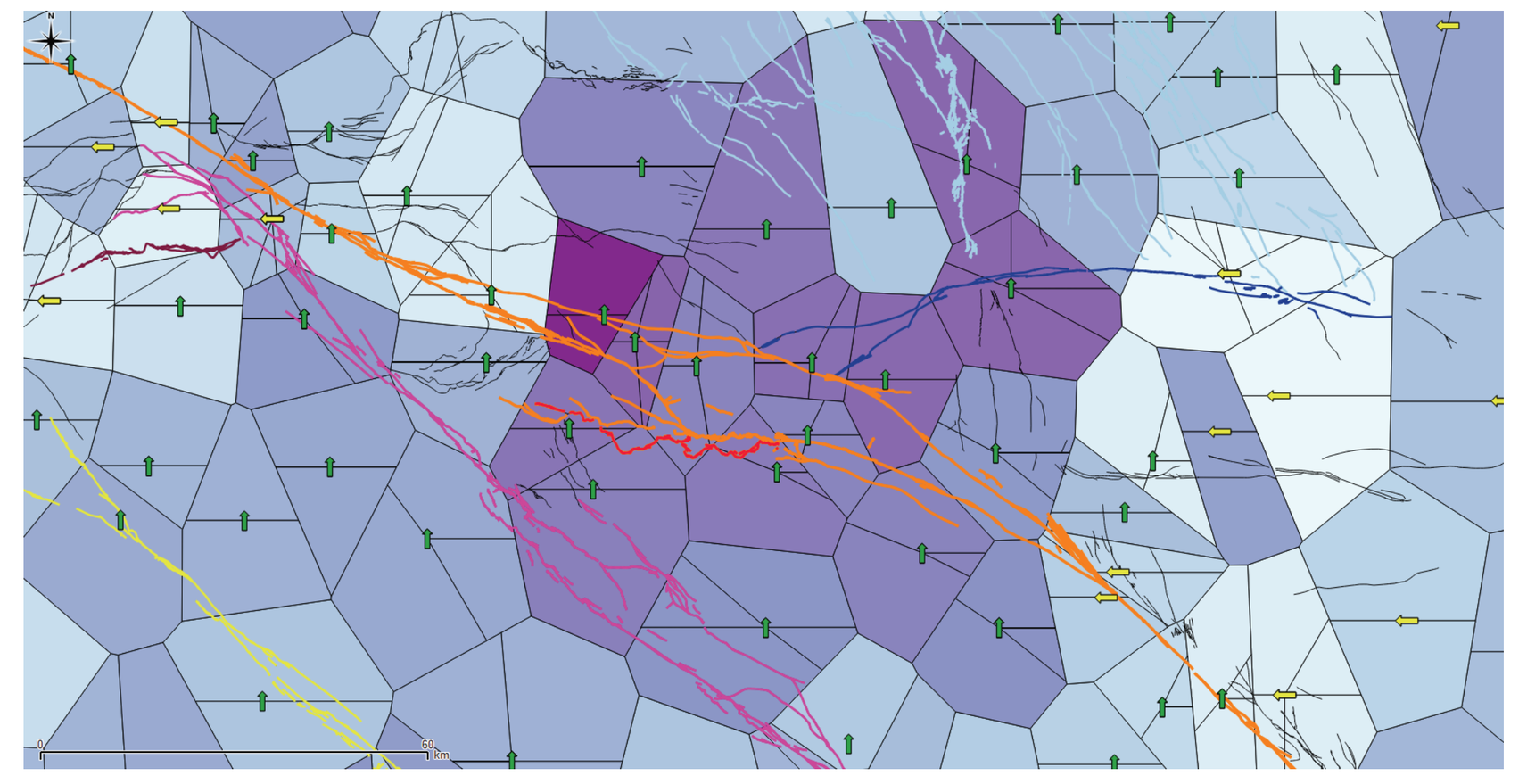

C.

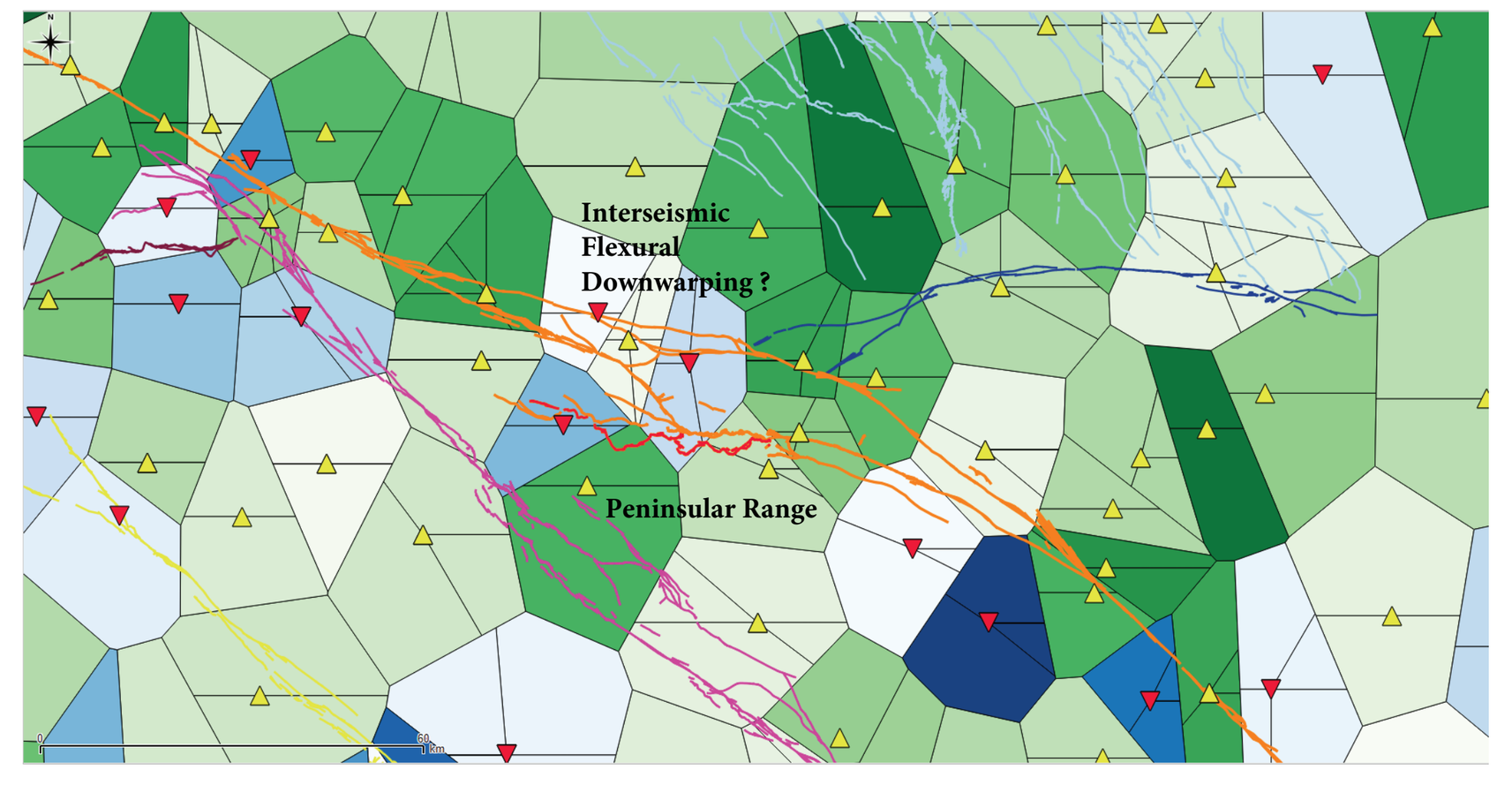

A. The difference (of the average) yellow and pea green velocities may may be considered the interseismic crustal velocity deficit for the Peninsular Range block (~6.5 mm yr^{-1}.) This deficit, if accrued over the observed RI of the SGP (~600-1000 yrs) yields ~ 4-6 m horizontal contraction per SGP seismic event. This value is similar in magnitude to the contraction determined independently in this study using CRN dating of deformed alluvial fans in Millard Canyon (~6-9m). The absence of the yellow velocity field also causes adjacency of orange and pea green fields, and therefore a steeper velocity field gradient. The location of this steep gradient is coincident with the San Jacinto fault (magenta in figure), suggesting a theoretical relationship between velocity field differences and fault slip, namely that faults accomodate differences in crustal velocities.

B. Geodetic northing and easting differentials at 1:500,000 scale. SGP region stands out as cluster of darker purple polygons indicating possible "torsion" (around z-axis) of geodetic station domain. Further analysis of these parameters may help with understanding fault behavior near vicinity of voronoi polygons boundaries.

C. Review of vertical geodetic components near SGP show what may appear to be contradictory arguments to the theory for contractional thrust faulting within the left stepover. However a reconsideration of this data illustrates what may be significant evidence of substantial interseismic strain accumulation in the hanging-wall and footwall blocks of the SGPF. The observed uplift (yellow triangles) within the Peninsular Range block may be recording the interseismic flexural warping as it (the footwall) is down-thrown. (See figure 16 Yule and Sieh, 2003). The two down-pointing red triangles in the headwall north of SGPF may very well be recording interseismic flexural downwarping due to shear forces caused by Peninsular Range block. This strain rebounds during the possible large magnitude ruptures through the SGP and manifests as fault scarps in alluvium. If this interpretation is true, the implications are for a possible large magnitude (Mw7+) Shakeout Scenario-type earthquake in the SGP and southern California.

B4 SCEC an NSF+USGS center

California State University Northridge

References

Balco G., Stone J., Lifton N., Dunai T., (2008) A simple, internally consistent, and easily accessible means of calculating surface exposure age and erosion rates from Be-10 and Al-26 measurements. Quaternary Geochronology 3, pp. 174-195.

Gosse, J., (2012) Dating techniques for surfaces and Quaternary sediments. Ed. C. Busby. "Recent advances in Tectonics of Sedimentary Basins", eds. C. Busby and A. Azor Perez, John Wiley and Sons. ISBN 13: 9781405194655. p. 63-79.

Jennings, C. W., (1994) Fault activity map of California and adjacent areas with location and ages of recent volcanic eruptions, Calif. Geol. Data Map Ser. Map 6, Calif. Dep. of Conserv., Div. of Mines and Geol., Sacramento.

Jones, L. M., (1995) Putting Down Roots in Earthquake Country, SCEC Spec. Publ..

Lal, D., (1991) Cosmic ray labeling of erosion surfaces: in-situ nuclide production rates and erosion models. Earth Planet. Sci. Lett. 104, 424–439

McBurnett, P., (2011) Paleoseimicity of the San Gorgonio Pass Fault Zone at the Millard Canyon: Testing the likelihood of a through-going San Andreas rupture [M.S. thesis]: California State University Northridge.

Petersen, M.D. and S.G. Wesnousky, (1994) Fault slip rates and earthquake histories for active faults in southern California, Bulletin Seismological Society of America, 84 no. 5, 1608-1649.

Ramzan, S., (2012) Paleoseismic Investigations of the San Gorgonio Pass Fault Zone Near Cabazon, California. n.p.: California State University, Northridge.

Sharp,R., (1975) Displacement on Tectonic Ruptures, CA Division of Mines and Geology bull. 196: San Fernando, California, Earthquake of 9 February 1971, Oakeshott, G., ed. pp. 187-194.

Spotila, J., K. Farley, and K. Sieh, (1998) Uplift and erosion of the San BernardinoMountains associated with transpression along the San Andreas fault, California, as constrained by radiogenic helium thermochronometry, Tectonics, 17,360–378.

Wesnousky, S.G., (1986) Earthquakes, Quaternary Faults and seismic hazard in California: Journal Geophysical Research, v. 91 p. 12587-12631.

Wolff, L. R., J D. Yule, K. M. Scharer, R. Witkosky, S. Ramzan, and P. McBurnett, (2014) Reconciling contradicting trench and geomorphologic observations across the San Gorgonio Pass Fault Zone. SCEC Abstract.

Yule, D., and K. Sieh, (2003) Complexities of the San Andreas fault near San Gorgonio Pass: Implications for large earthquakes, J. Geophys. Res., 108(B11), 2548, doi:10.1029/2001JB000451.

Yule et al., (2015) Frequency of Plausible, Worst-Case Scenario Earthquakes on the southernmost San Andreas Fault. Abstract: this meeting.

Special Thanks to: Lisa Wolff, Ryan Witkosky, Paul McBurnett, and Shahid Ramzan for previous work in SGP area, Jose Cardona for help with sample processing, and Kate Scharer for directing regional earthquake science research in the public interest. Thanks to Bob Finkel and Susan Zimmerman at LLNL for providing top-quality AMS data.

This research was funded by SCEC 2012 project 12209
Focus Area: SoSAFE, and WGCEP.

Any Questions/Comments?
email: ian.desjarlais@csun.edu